

Featuring work from the Laboratory for Functional Tissue Engineering research group of Prof. Milica Radisic, University of Toronto, Canada. Andrea Lam is acknowledged for the cover design.

Curvature facilitates podocyte culture in a biomimetic platform

Biomimetic “bubbly” topography, fabricated using SU8 and glass bead molding, offers the relevant microcurvature for kidney podocyte cells to wrap around and to facilitate differentiation during culture.

As featured in:



See Milica Radisic, Boyang Zhang et al., *Lab Chip*, 2018, 18, 3112.



Cite this: *Lab Chip*, 2018, 18, 3112

Curvature facilitates podocyte culture in a biomimetic platform†

Anastasia Korolj,^a Carol Laschinger,^b Chris James,^c Erding Hu,^c Claire Velikonja,^a Nathaniel Smith,^a Irene Gu,^a Samad Ahadian,^b Robert Willette,^c Milica Radisic^{*abde} and Boyang Zhang^{id}^{*b}

Most kidney diseases begin with abnormalities in glomerular podocytes, motivating the need for podocyte models to study pathophysiological mechanisms and new treatment options. However, podocytes cultured *in vitro* face a limited ability to maintain appreciable extents of differentiation hallmarks, raising concerns over the relevance of study results. Many key properties such as nephrin expression and morphology reach plateaus that are far from the *in vivo* levels. Here, we demonstrate that a biomimetic topography, consisting of microhemispheres arrayed over the cell culture substrate, promotes podocyte differentiation *in vitro*. We define new methods for fabricating microscale curvature on various substrates, including a thin porous membrane. By growing podocytes on our topographic substrates, we found that these biophysical cues augmented nephrin gene expression, supported full-size nephrin protein expression, encouraged structural arrangement of F-actin and nephrin within the cell, and promoted process formation and even inter-digitation compared to the flat substrates. Furthermore, the topography facilitated nephrin localization on curved structures while nuclei lay in the valleys between them. The improved differentiation was also evidenced by tracking barrier function to albumin over time using our custom *topomembranes*. Overall, our work presents accessible methods for incorporating microcurvature on various common substrates, and demonstrates the importance of biophysical stimulation in supporting higher-fidelity podocyte cultivation *in vitro*.

Received 14th May 2018,
Accepted 4th September 2018

DOI: 10.1039/c8lc00495a

rsc.li/loc

Introduction

A major bottleneck in the study and treatment of glomerular diseases is that podocytes cultured *in vitro* do not sufficiently resemble their typical *in vivo* characteristics. Podocytes are highly specialized, terminally differentiated epithelial cells that wrap around glomerular capillaries.¹ They provide barrier function for filtration of the roughly 1 liter of blood that passes through the kidneys every minute.² A very high extent of differentiation and structural conformity is required for these cells to perform their required function.³ In fact, impairment in podocytes (*e.g.* effaced foot processes⁴) or in their microenvironment (*e.g.* thin basement membrane^{5,6}) usually leads to the breakdown of kidney function in general.

An overwhelming majority of diseases that progress to chronic kidney disease (CKD) begin with glomerular podocytes, due in major part to the inability of podocytes to repair, replicate or regenerate after injury.⁷ If in a given glomerulus the number of podocytes drops below 60% of the normal number, the entire nephron will be lost.^{4,8} As progressively more nephrons are lost, filtration function gradually diminishes and CKD advances until end-stage renal disease (ESRD), when the kidneys have fully failed and a patient must rely on dialysis or a kidney transplant to survive.⁹ It is estimated that one in seven people are affected by CKD, and three-quarters of transplant waitlists around the world are for kidneys.^{10–12} In addition, approximately 20% of nephrotoxicity is drug-induced, with that number rising to over 60% in elderly populations.^{13,14} Thus, adverse drug reactions are a concern for the kidneys, with around 4% of drug withdrawals from the market being due to renal toxicity.¹⁵ *In vitro* tools for studying podocyte pathogenesis are needed to discover new treatments and potential mechanisms of repair or regeneration of filtration function, as well as for more sensitive screening of early adverse effects of drugs on podocytes, for which there is a shortage of clinical markers.

Current progress towards developing *in vitro* models of podocytes is promising. Immortalization of murine and

^a Department of Chemical Engineering and Applied Chemistry, University of Toronto, Canada. E-mail: m.radisic@utoronto.ca

^b Institute of Biomaterials and Biomedical Engineering, University of Toronto, Canada. E-mail: by.zhang@utoronto.ca

^c GlaxoSmithKline, Heart Failure Discovery Performance Unit, King of Prussia, PA, USA

^d Toronto General Research Institute, University Health Network, Toronto, Canada

^e The Heart and Stroke/Richard Lewar Center of Excellence, Toronto, Canada

† Electronic supplementary information (ESI) available. See DOI: 10.1039/c8lc00495a

human cell lines have provided an abundant source of cells, including lines harboring genetic mutations that correspond to patient diseases.^{16–19} Development of pluripotent stem cell-derived podocytes could also serve as an unlimited cell source and pave the way to patient-specific modeling.^{20–22} However, cultured podocytes face limited ability to maintain an appreciable extent of differentiation hallmarks, raising concerns over the relevance of study results.^{23,24} Many key properties such as nephrin expression and morphology reach plateaus that are far from the *in vivo* levels.^{25–27} Several techniques have been explored to enhance differentiation of cultured podocytes, including co-cultures,^{28,29} biochemical supplementation,^{27,30,31} and stretch,^{21,32,33} stiffness,³⁴ and flow modulation.^{21,35,36} Such biophysical cues are known to affect and enhance *in vitro* cell and tissue cultures.^{37,38} However, a question that has up to this point remained unanswered is how the physical shape of the microenvironment contributes to the integrity of podocytes in a robust cell culture system.

In the glomerulus, podocytes wrap around a dense cluster of looping capillaries, forming an expansive three-dimensional mesh (Fig. 1a).³⁹ Primary processes extend out radially from a large cell body, and further branch into fine foot processes, supported by the actin cytoskeleton (Fig. 1b).⁴⁰ These foot processes interdigitate with those of adjacent podocytes (Fig. 1c)⁴⁰ to form nephrin-rich slit diaphragms, which are the transmembrane protein complexes responsible for barrier function. The result is an intricate 3D structure that is critical to proper podocyte function. We hypothesized that a biomimetic topography, that mimics the curvature of glomerular capillaries, would provide a physical stimulus that promotes podocyte differentiation *in vitro*.

In this work, we first demonstrate novel techniques for incorporating microcurvature onto various substrates, including thin porous membranes. We then demonstrate the physiological effects of this geometric stimulation in promoting podocyte differentiation, by assessing the upregulation of nephrin gene expression, protein expression and localization, development of cytoplasmic cell processes, and barrier function, with results highlighted in contrast to biochemical stimulation.

Experimental

Platform fabrication

Glass beads (<100 μm , G4649 Sigma-Aldrich) were poured onto the entire surface of a silicon wafer spin-coated with an SU-8 2050 seed layer (50 μm thick) (Fig. 1d, i). The surface was then exposed to UV irradiation, thereby locking the glass beads together with the SU-8 onto the wafer (Fig. 1d, ii). This master was then used to create an inverse mold with concave microhemispheres out of polydimethyl siloxane (PDMS) (Fig. 1d, iii). The PDMS inverse mold was plasma bonded against another silicon wafer, fully cured at 120 $^{\circ}\text{C}$ and used as the master mold to make a PDMS replicate of the bubble surface with out-of plane microhemispheres (Fig. 1d, iv). Circular inserts were punched out from the bubble surface, autoclaved, and

then placed into the 24-well plate, thereby creating a transformed cell culture plate for podocytes (Fig. 1d, v).

Profilometry

To quantify the heights, diameter, and coverage of the bubbles on the PDMS bubble surfaces, we used a profilometer (KLA-Tencor P16+ Surface Profilometer at the Ontario Centre for the Characterisation of Advanced Materials, University of Toronto, Canada). Multiple horizontal profiles at fixed vertical separations were measured, leading to the mapping of a 2D surface. We characterized five 400 by 400 μm squares from 3 PDMS bubble inserts, with a resolution of 4 data points per μm in the x-axis and 1 data point per μm in the y-axis. The resulting profile maps (Fig. 1e) were analysed in ImageJ using the “Analyze Particles” feature. This provided the diameter of each bubble, as well as the percent area that was covered by bubbles. In addition, the maximum grey value per bubble was measured, which was used to calculate each bubble's height by correlating it to the grey values of the elevation scale bar (produced by the profilometer) (Fig. 1f–h).

Hot embossing

The hemispherical microfeatures of our PDMS mold were transferred to a 1.4 mm thick sheet of clear polystyrene in a hot embosser, using a force of 500 N and temperature of 180 $^{\circ}\text{C}$ for 20 minutes. The polystyrene sheet, now containing convex hemispherical microfeatures, was cut into a smaller rectangle (85 by 127 mm) in order to fit the base of a 24-well bottomless plate from Greiner Bio-One $\text{\textcircled{c}}$. To bond the base to the bottomless plate, the hot embosser pressed the two parts together with a force of 200 N for 6 minutes, at temperatures of 122 $^{\circ}\text{C}$ (to the base) and 80 $^{\circ}\text{C}$ (to the top of the well plate) (Fig. S1a \dagger). The result was a 24-well topographic plate ready for cell culture (Fig. S1b \dagger). To demonstrate the translatability of the polystyrene cell culture plate to culture applications, we coated the bottoms of the wells with Matrigel prior to cell seeding, using the same procedure as with the inserted PDMS platforms. Podocytes were grown under differentiating conditions in supplemented culture media. Samples were stained and imaged (Fig. S1c \dagger).

Cell maintenance

E11 murine podocytes (a kind gift from GSK, also available from BioCat) are a conditionally immortalized cell line, and are grown under different conditions to encourage the proliferative *versus* differentiating stages.⁴¹ Cells were first grown under conditions permissive to proliferation in order to generate a higher cell number prior to differentiation experiments. The podocytes were plated in a collagen I coated T175 flask in proliferation media: RPMI 1640 media containing GlutaMAX and HEPES, with added 10% (v/v) fetal bovine serum (FBS), 1% (v/v) penicillin–streptomycin (pen-strep), and supplemented with 10 units per mL recombinant murine interferon gamma. Podocytes were grown at 33 $^{\circ}\text{C}$ until 80% confluent. Then podocytes were either trypsinized and collected for seeding the experiment or moved to differentiation

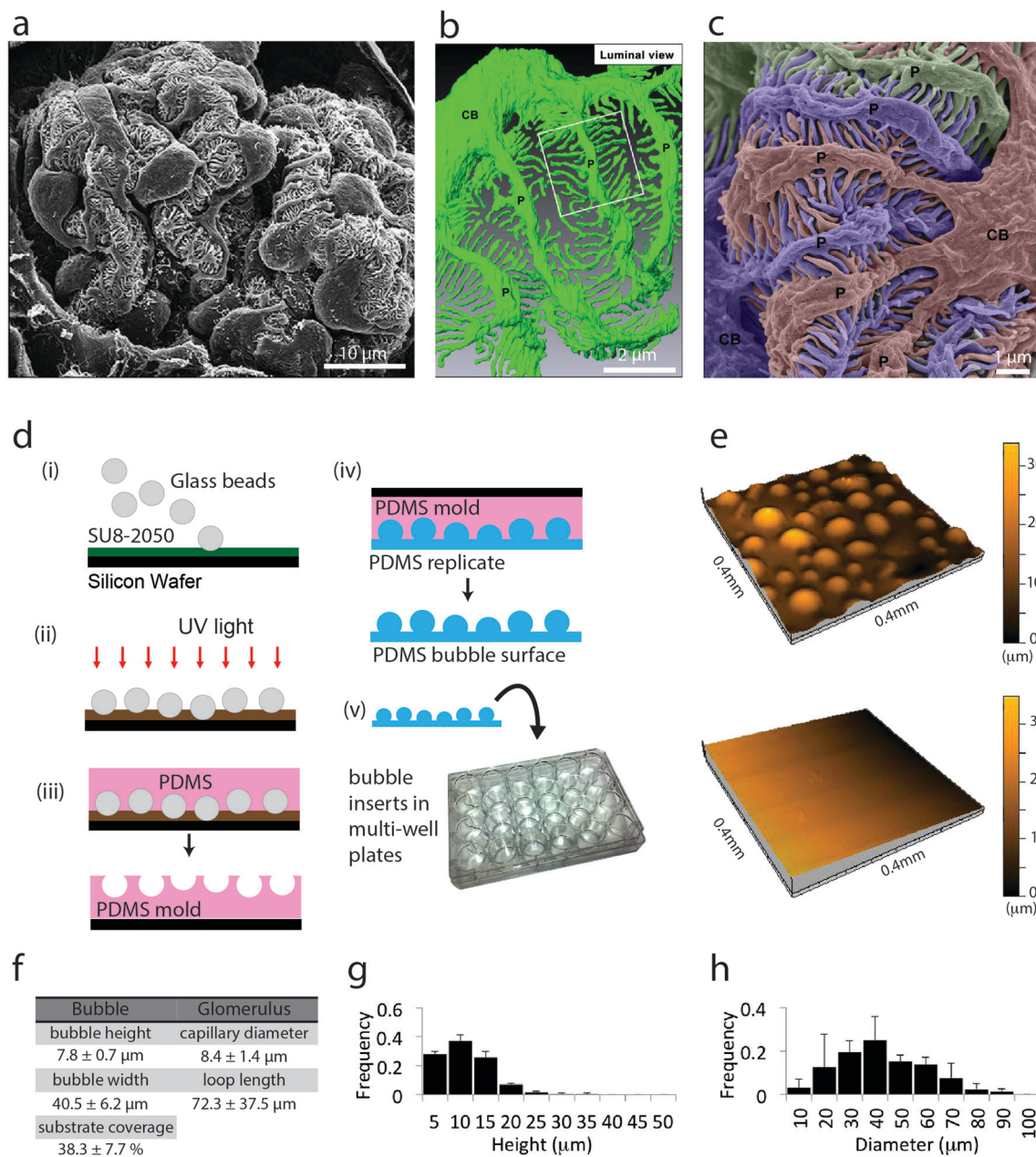


Fig. 1 The biomimetic bubble substrate for podocyte cultivation is inspired by the structure of the native glomerulus. (a) Scanning electron micrograph (SEM) of a native glomerulus with supporting capillaries. *Reproduced with permission from The Company of Biologists.*³⁹ (b) SEM image of a single podocyte, and (c) Pseudo-colored SEM image showing interdigitated podocytes in a native glomerulus. *Reproduced with permission from Springer Nature.*⁴⁰ (d) Schematics of the modified photolithography and micromolding process used to prepare the micro-hemispherical “bubble” topography. (i) Micro-glass beads were sprinkled over an SU8-coated silicon wafer, then (ii) exposed to UV light to fix the glass beads in place. (iii) Glass bead-covered wafer was molded with PDMS to create an inverse master mold. (iv) Inverse master mold was molded again to create PDMS replicates of the bubble surface. (v) The replicated PDMS bubble surface was punched into well-size substrates which were then inserted into a 24-well plate. (e) Profilometry of the bubble and flat substrates for podocyte cultivation. (f) Quantification of bubble features on the topographic substrates and comparison to the dimensions of *in vivo* rat glomerular capillaries.^{43,44} Histograms of the bubble features’ (g) height and (h) diameter. $n = 5$ images analyzed from $n = 3$ /group.

conditions. Unless otherwise stated, cell culture materials were obtained from Thermo Fisher Scientific.

Cell seeding and culture on platform

Prior to experiments, the PDMS inserts were autoclaved and coated with Matrigel (1 : 60 dilution from 9.3 mg mL^{-1} stock so-

lution) for 2 hours. On day 0, cells were seeded with proliferation media at low or high seeding density (15 000 cells per cm^2 or 50 000 cells per cm^2 , respectively) on either a topographic or a flat platform (in the 24-well plate described above) and transferred to 38°C to begin differentiation. Cells were allowed to attach for one day, and then on day 1 the culture media was changed to differentiation media: DMEM-F12 basal media

(Life Technologies) containing 10% (v/v) FBS, and 1% (v/v) pen-strep. Select biochemical supplementation was applied as follows. Three media groups were compared: (1) unsupplemented (vehicle only) differentiation media, (2) all-*trans*-retinoic acid (ATRA, Sigma-Aldrich) and, (3) dexamethasone (DEX, Sigma-Aldrich). The ATRA group consisted of differentiation media and 10 nM 1,25-dihydroxyvitamin D3 (Vit D3, Enzo Life Sciences) and 200 nM ATRA. The DEX group was identical to the ATRA group but had an additional 100 nM DEX included for the first 48 hours of supplemented culture, with its use discontinued on day 3 of the culture process. Media was changed every other day until cells were either harvested for RNA isolation and gene expression analysis, or fixed for imaging (Fig. 2a).

Relative gene expression quantification

On day 9, cells were washed with warm, non-supplemented RPMI 1640 basal media prior to lysing and RNA isolation. A High Pure RNA Isolation Kit (Roche) was used according to manufacturer's instructions, using 50 μ L of elution buffer for the final step. Each sample from the experiment consisted of 3 individual wells pooled together, to ensure that a sufficient amount of RNA was being collected. Thus, 9 wells were seeded for each group to generate $n = 3$ samples per condition. Isolated RNA was converted to complementary DNA (cDNA) using the high capacity cDNA reverse transcription kit (Applied Biosystems) for ensuing PCR ap-

plications. RNA solutions were diluted to a final 7.5 ng μ L⁻¹ in a total reaction volume of 60 μ L. Real-time PCR was run on the generated cDNA using the TaqMan Gene Expression Assay (Applied Biosystems). cDNA was diluted to 3.33 ng μ L⁻¹ in a volume of 9 μ L, for a total of 30 ng cDNA per reaction. Taqman assays were run on a qPCR Lightcycler 480 (Roche) according to the following PCR conditions: incubation at 95 °C for 10 min, 55 cycles of 95 °C for 15 s, 60 °C for 1 min, and 72 °C for 1 s. Expression of murine nephrin gene (NPHS1, Thermo Fisher Scientific) and the housekeeping gene beta-2-microglobulin (B2M, Thermo Fisher Scientific) was determined using relative quantification analysis, where C57/bl6 mouse whole kidney cDNA was used as a positive control and as a normalizer in calculations (Fig. 2b and c). Note that data in Fig. 2 and 6 were normalized to different batches of mouse whole kidney cDNA control samples and thus are relative.

Western blot

Cells cultured for over 14 days on flat and bubble substrates under DEX supplementation were washed with ice-cold Dulbecco's phosphate buffered saline (PBS, Life Technologies) and lysed in RIPA buffer with protease inhibitors. Lysates were centrifuged at 12 500 rpm for 15 minutes and protein concentrations were determined by bicinchoninic acid protein assay kit (Pierce). 20–30 μ g of total protein were resolved by SDS-PAGE using Bolt™ 4–12% Bis-Tris Plus gels (ThermoFisher Scientific) and transferred to PVDF

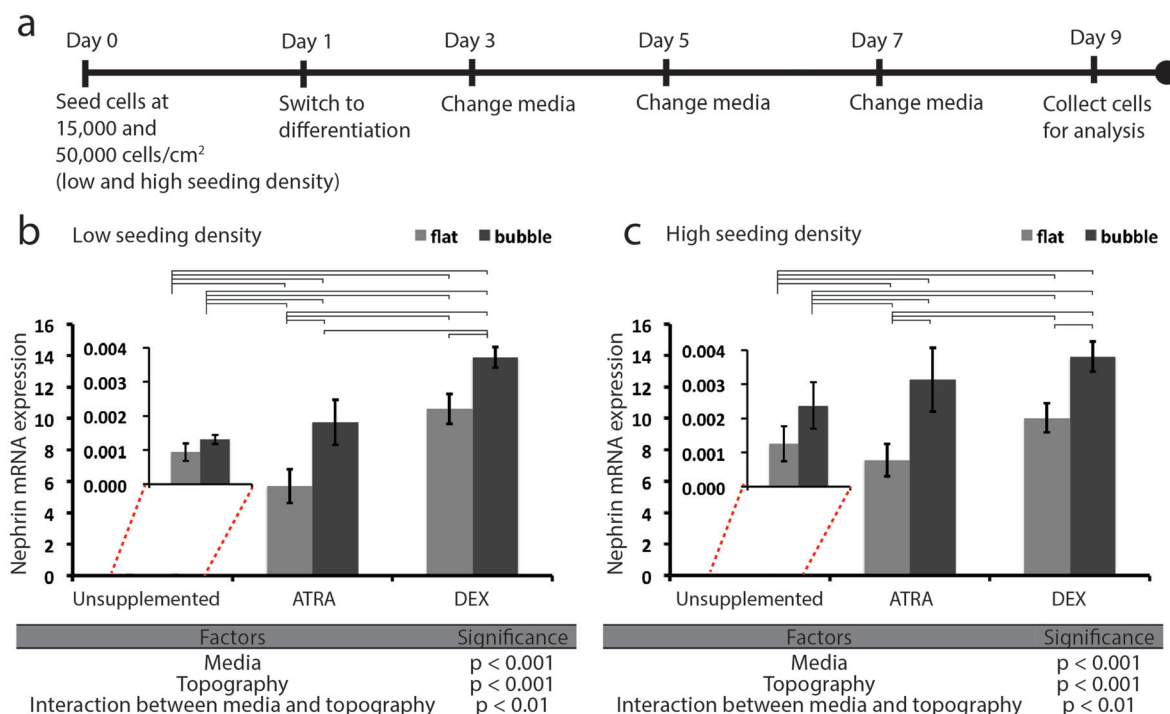


Fig. 2 Relative nephrin gene expression is increased for podocytes grown on the bubble substrate compared to the flat substrate. (a) Timeline showing experiment protocol. Relative nephrin gene expression for cells seeded at (b) low density (15 000 cells per cm^2) and (c) high density (50 000 cells per cm^2). ATRA indicates culture media supplemented with 200 nM all-*trans* retinoic acid and 10 nM dihydroxy-vitamin D3, and DEX indicates culture media supplemented with an additional 100 nM dexamethasone for the first 48 hours of culture. Data is average \pm s.d., $n = 3$. Lines indicate significant difference between groups with $p < 0.05$. Tables show results of 2-way ANOVA.

membranes. Immunoblotting was performed using primary HRP-tagged monoclonal nephrin and GAPDH antibodies (Santa Cruz) overnight at 4 °C, then washed and imaged using ECL blotting reagents and ImageQuant LAS500 (GE). Blot quantitation was performed using ImageJ's "Analyze Gels" tools (Fig. S6†).

Immunofluorescent staining and confocal imaging

For immunofluorescent staining (Fig. 3, 4a, and S2 and S5†), cells were first washed with PBS and then fixed in 4% paraformaldehyde solution for 15 min at room temperature, followed by another wash with PBS. For nephrin and wheat germ agglutinin (WGA) staining (Fig. 3), the cells were blocked in 10% normal goat serum in PBS for 1 hour. Next, the cells were incubated in primary anti-nephrin antibody (Thermo Fisher Scientific) overnight at 4 °C followed by incubation with FITC goat anti-rabbit IgG (1:200 dilutions, Abcam) for 1 hour at room temperature. Lastly, the cells were incubated with Rhodamine-WGA (1:1000 dilution, Vector Laboratories) for 10 min at room temperature. For F-actin staining (Fig. 4a and S5†), the cells were permeated and blocked in 10% (v/v) FBS and 0.25% Triton X100 in PBS for 1 hour. Next, the cells were incubated with Alexa Fluor® 660 phalloidin (Thermo Fisher Scientific) for 1 hour. Samples were imaged with confocal microscopy, using a Nikon A1R+ resonance scanning confocal microscope at the Advanced Optical Microscopy Facility at Toronto General Hospital. Groups of images were taken in the same sitting with consistent image acquisition settings.

Immunofluorescence quantification

Confocal immunofluorescent z-stack images were analyzed using ImageJ. Maximum intensity z-projections of three image channels were used and raw integrated density values were recorded. To compare outer to central nephrin (Fig. 3b and S3†), regions corresponding to nuclei were found and stored to the region of interest (ROI) manager using the "Analyze Particles" feature. These regions were then selected on the image corresponding to the nephrin channel, and nephrin signal within (*i.e.* central) and outside (*i.e.* outer) the selected nuclei regions was collected. A ratio was computed to quantify the distribution of nephrin in the center *versus* in the cell periphery by dividing outer by central nephrin, where a higher ratio indicates that a greater proportion of nephrin was found outside the nuclear regions. For quantification and localization of nephrin and nuclei relative to the bubble structures (Fig. 3e–g and S4†), brightfield overlay images of the substrate were compared with stained images to delineate the different substrate regions.

Scanning electron microscopy

Fixed cells on the platforms were washed 3 times with PBS, then post-fixed with 1% osmium tetroxide (in PBS) for 10 minutes at room temperature in the dark. Then, samples were washed again 3 times with PBS, and then dehydrated in the

24-well plates in a serial ethanol wash over a course of 2 hours, in five steps going from 25% to 100% ethanol in PBS. After ethanol dehydration, the PDMS platform inserts with cells were removed from their wells and sliced into quarters for critical point drying. The samples were dried at the critical point, and sputter-coated with gold before scanning electron microscopy (SEM) imaging on a Hitachi S-3400N scanning electron microscope (Fig. 4b–d and S7†).

Cell process quantification

SEM images were used for quantifying podocyte processes. In ImageJ, the segmented line tool was used first to measure the scale bar, and then to trace and measure the boundary length and the digitated length of a cell boundary (Fig. 4d). The boundary length refers to the cell boundary line, perpendicular to the protruding processes from that boundary. The digitated length refers to the length of the perimeter traced around all the protruding processes within that boundary. The digitation ratio is obtained by dividing the digitated length by the boundary length (Fig. 4e). The average length of processes was approximated by dividing the digitated length by the boundary length, and again by 2 (to account for the perimeter which measures each side of a protrusion) (Fig. 4f). Process density (Fig. 4g) represents the number of processes counted per 1 μm of boundary length. The same was repeated for control samples in Fig. S7.† SEM images of podocytes on the native glomerulus were also collected from the literature^{39,40,79–81} and quantified in the same way to provide an approximate "in vivo" range of process quantification parameters.

Membrane fabrication

A 50 μm layer of SU-8 2050 was spin coated onto a silicon wafer (Fig. 5a, i). It was baked on a hotplate at 95 °C for 2–3 minutes, then a PDMS replica of the bubble topography was imprinted on the gelled SU-8 layer and allowed to further solidify at 65 °C (Fig. 5a, ii). After cooling, the PDMS replica was peeled off and UV-cured, revealing a negative copy of the bubble topography (Fig. 5a, iii). A 25 μm layer of SU-8 2025 was spin coated onto the indented wafer, taking care to avoid bubble formation (Fig. 5a, iv). This layer was exposed through a photomask with an array of holes (Fig. 5a, v). Development of the master revealed a negative topography space filled with micropillars (Fig. 5a, vi). These micropillars provided pores for increased permeability of the resultant membrane. To fabricate the membrane, PDMS was spin coated onto the master at 3000 rpm for 5 minutes (Fig. 5a, vii). The cured PDMS was swelled with diethyl ether, then washed in water, and bored into circles the size of a Transwell® membrane (Fig. 5a, viii). Transwell® inserts, with the original membrane removed, were coated with a thin layer of PDMS before placing onto the round topomembranes (Fig. 5a, ix). Curing the membrane to the insert resulted in rapid and reproducible assembly of

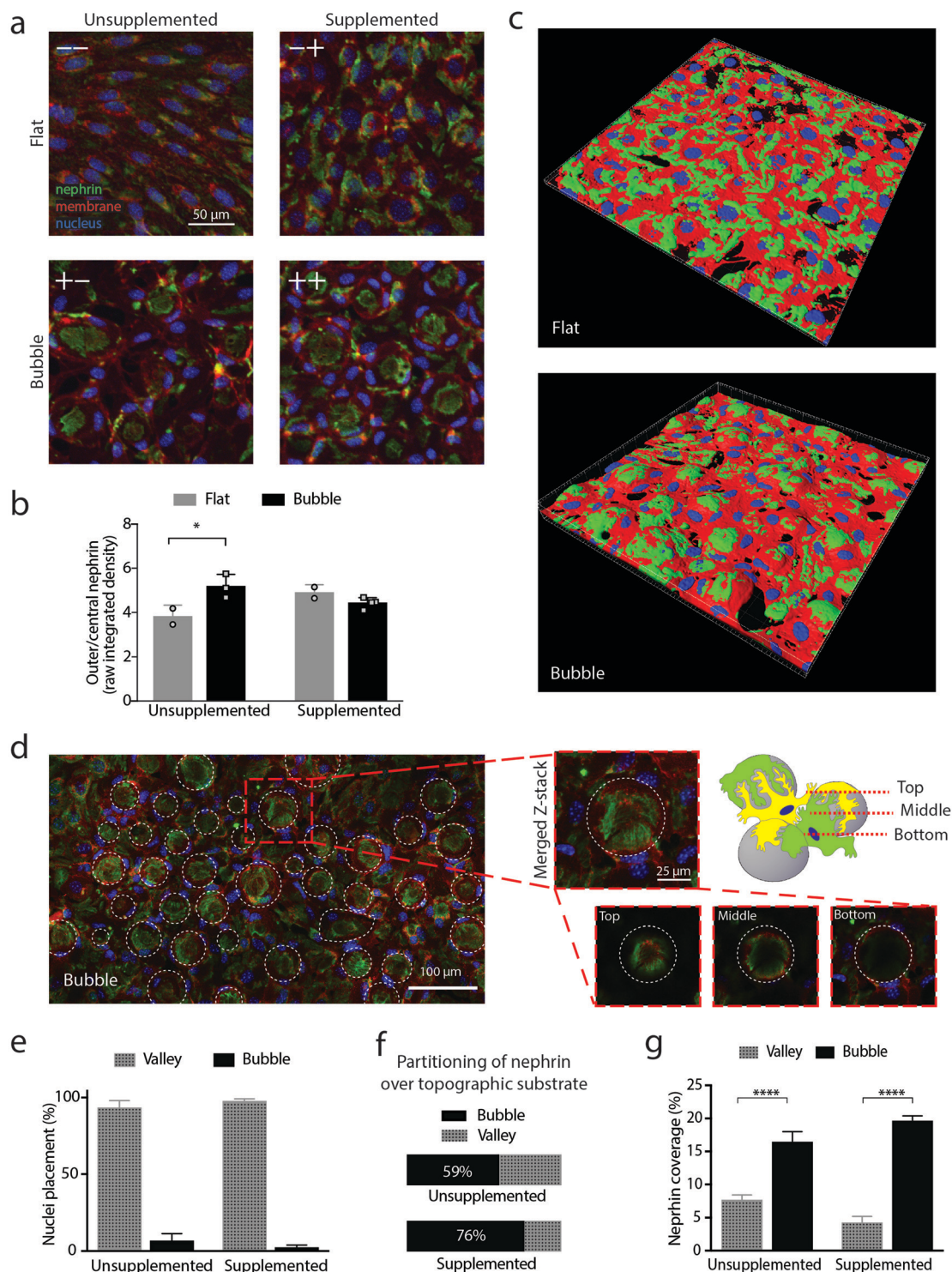


Fig. 3 Biochemical and topographical stimulation influence nephrin localization in the cell. (a) Immunofluorescent staining for nephrin (green), WGA (red), and DAPI (blue). -- no stimulation, - + biochemical stimulation, + - topographical stimulation, ++ both stimuli. (b) Ratio of nephrin in outer to central regions of the cell, with high values indicating localization in cell periphery. (c) 3D reconstructions of confocal immunofluorescent microscopy of podocytes on flat and bubble substrates stained for nephrin (green), WGA (red), and DAPI (blue). (d) Confocal z-stack through a single bubble structure reveals that nephrin is located along the surface of the bubble, whereas nuclei and cell bodies remain in valleys. Within the topographic substrate: (e) percentage of nuclei located in valleys or on bubble structures, in the field of view. (f) Partitioning of the total nephrin from the field of view into either valley or bubble structure areas. (g) Percentage of the surface covered by positive nephrin staining within the surface type. $n = 2-5$ sample images per group. Averages \pm s.d. are shown. * $p < 0.05$, **** $p < 0.0001$.

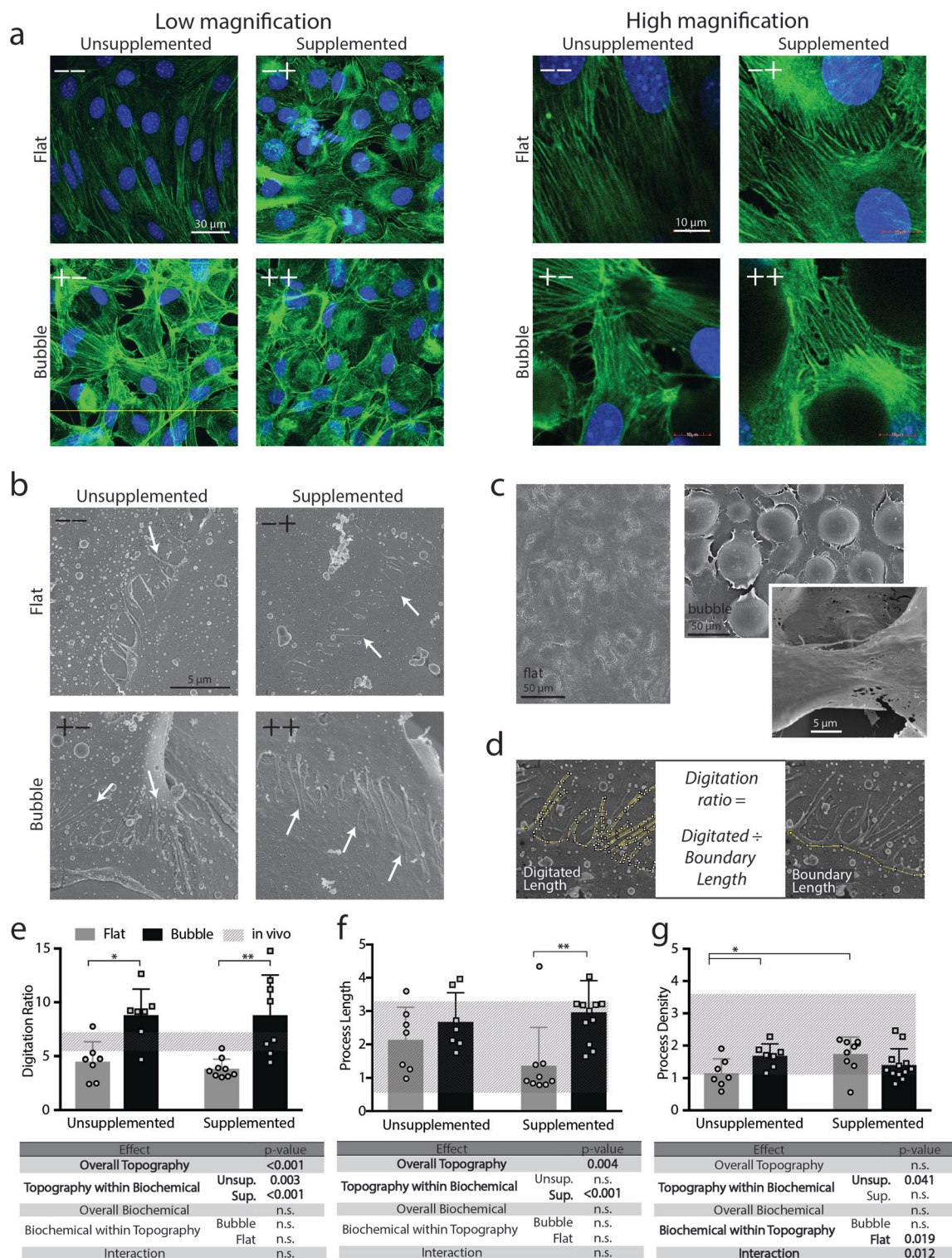


Fig. 4 Cultivation on the bubble surface promotes extension of processes in podocytes. (a) F-actin staining at low and high magnifications. (b) SEM reveals the formation of cell processes. White arrows indicate locations of processes. (c) SEM reveals extension of podocyte processes between the tops of two adjacent bubble structures, unique to the bubble substrate. (d) The digitation ratio is defined as the digitated length over the boundary length. Quantification of (e) digitation ratio, (f) average process length, and (g) average process density defined as the number of processes per micrometer of boundary length. Shaded areas correspond to the equivalent average \pm s.d. for each parameter calculated for the *in vivo* case, from SEM images in the literature. $n = 10$ images of cell-cell boundaries per group from $n = 3$ samples, average \pm s.d. shown. Statistics using two-way ANOVA are indicated in the tables. * $p < 0.05$, ** $p < 0.01$.

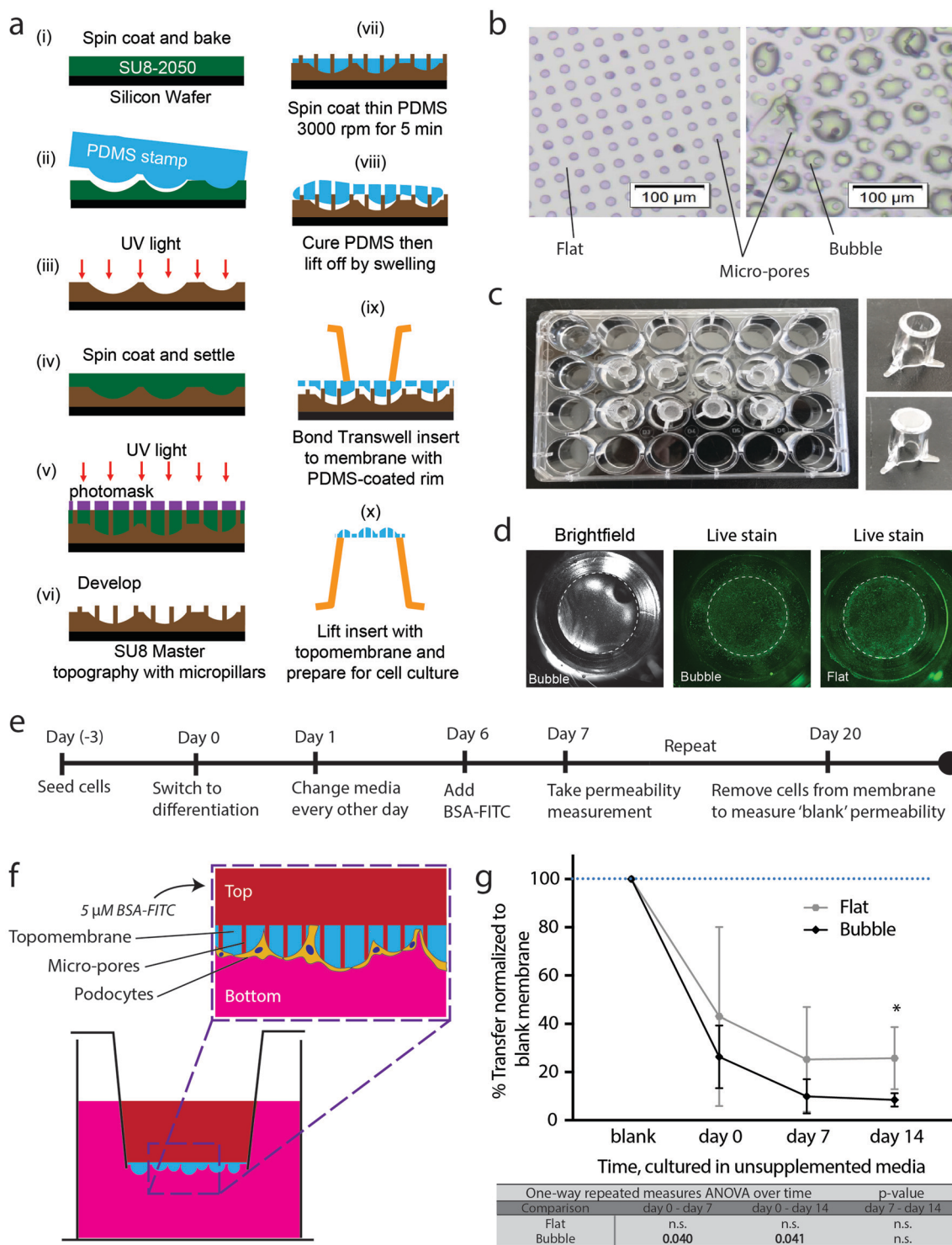


Fig. 5 Topomembrane enables quantification of podocyte barrier function. (a) Schematics of the modified photolithography and molding processes used to prepare a permeable bubble membrane. (i) Silicon wafer was spin coated with SU8, then (ii) stamped to create (iii) a dimpled layer, onto which (iv) a second SU8 layer was (v) patterned with micropillars. (vi) The dimpled micropillar master was used with (vii) spin-coated PDMS to create a thin microporous and bubbled PDMS membrane which was (viii) swelled to detach from the master and (ix) cured onto the rim of a transwell insert. (x) Lifting off the insert with the PDMS membrane yields the final topomembrane. (b) Brightfield images of the flat membranes and topomembranes. (c) Custom topomembranes inserted into standard 24-well plate. (d) Brightfield and fluorescent live-stained (green, CFDA-SE) images of cells covering the membrane area. (e) Timeline for topomembrane cell culture and permeability experiment. (f) Schematic of the topomembrane setup. (g) Barrier function expressed as percent transfer across the topomembrane, measured for flat membranes and topomembranes over time. (*) indicates significant difference ($p < 0.05$) on day 14 between flat and bubble groups by unequal variances *t*-test. Statistics for one-way repeated measures ANOVA over time within each group are shown in the table. $n = 3$ inserts for bubble and $n = 5$ for flat group.

custom topomembranes (Fig. 5a, x). Resultant flat and topomembranes had arrays of through-holes (Fig. 5b) and could be used for Transwell cell culture experiments (Fig. 5c and d). Defects such as membrane wrinkling or incomplete attachment to the insert perimeter were discarded from the experiment. Membranes were also fabricated by injection molding of POMaC between PDMS copies of the membrane mold and a glass slide (Fig. S8†).

Cell seeding and culture on membrane

Prior to cell culture, membranes were washed and sterilized in a series of alternating 70% ethanol and PBS baths over the course of 6 hours. Matrigel in a 1:60 dilution in basal medium was used to coat the membranes by immersion. Cells were seeded on the underside of the insert on day (-3) by placing inserts upside-down in 12-well plates, and pipetting 60 μ L of cell suspension onto the membrane. Cells were incubated and allowed to attach for 3 hours before replacing inserts into regu-

lar 24-well plates. Cells on the topomembranes were monitored and allowed to proliferate for roughly 3 days until 85% confluent on the membranes, at which point the incubator temperature was changed to 38 °C (start of day 0) and media was changed to unsupplemented differentiation media (Fig. 5e).

Permeability measurements

Stock solution of 66 kDa bovine albumin-FITC (Sigma-Aldrich) was prepared at 55 μ M in culture medium. For each permeability measurement, 10 μ L of the stock solution was pipetted into the 100 μ L topomembrane insert, giving a starting concentration of 5 μ M in the upper “blood” chamber (Fig. 5f). After 30 hours of diffusion time, 80 μ L of solution was sampled from the top and from the bottom wells, then fluorescence was measured with a SpectraMAX plate reader. Fluorescence readings were correlated to concentration using a standard curve that went through the origin. Percent transfer was calculated by dividing the bottom by the top well

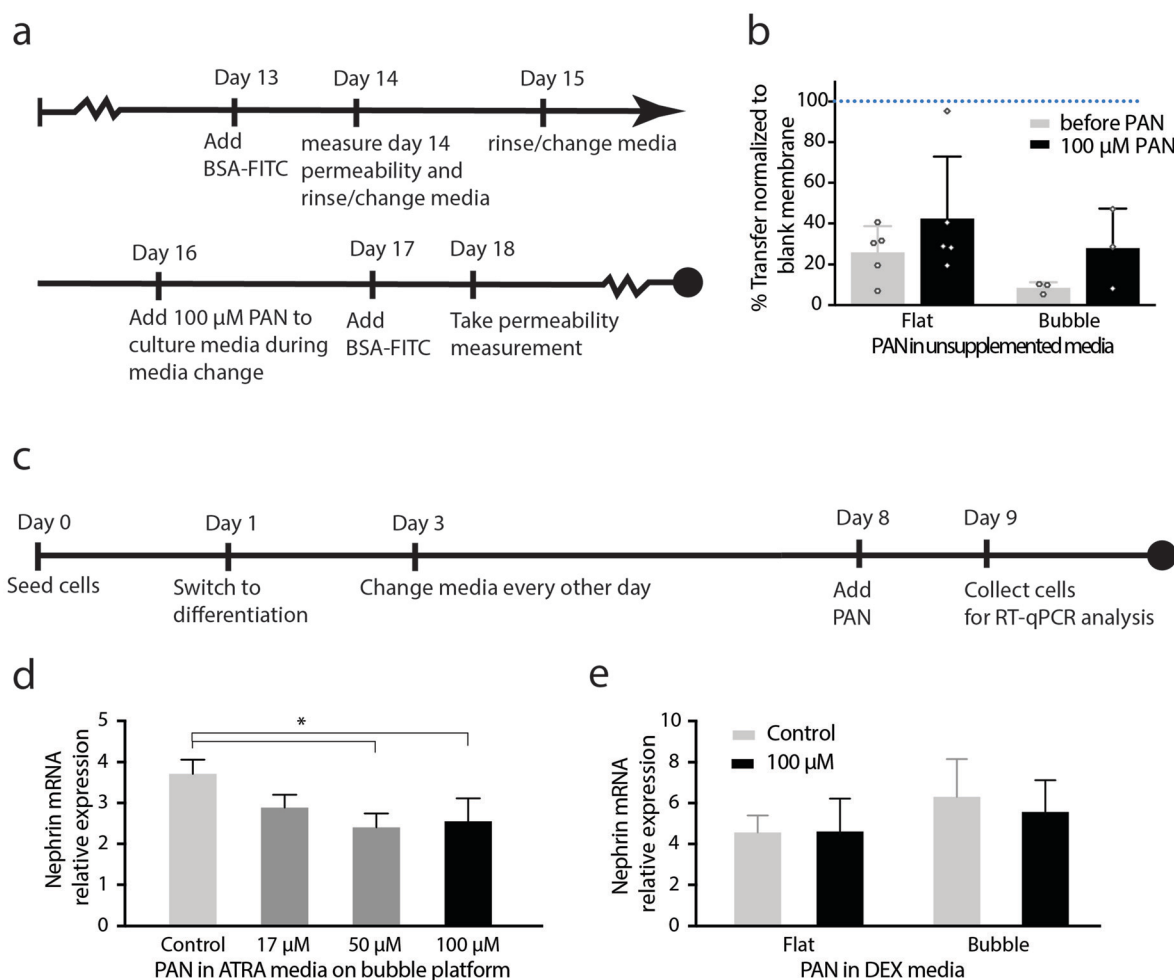


Fig. 6 The bubble substrates model effects of drug-induced injury. (a) Timeline for puromycin aminonucleoside (PAN) injury experiment on the flat and topomembranes in unsupplemented media. (b) The effect of PAN on barrier function measured as percent transfer of FITC-labelled albumin across the podocyte-covered topomembrane. (c) Timeline showing administration of PAN to podocyte cultures on the bubble substrate. (d) Relative nephrin gene expression at different doses of PAN, in culture media supplemented with ATRA on the bubble substrate. (e) Protective effect of dexamethasone (DEX) supplement is observed for relative nephrin gene expression on both flat and bubble substrates. * $p < 0.05$.

concentrations. At least 2 washes (media changes) over 3 days were allowed between permeability measurements, to wash out residual dye. Dye is only added on days in between media changes, to allow culture media to equilibrate in the wells, thereby preventing convective flow between the top and bottom compartments. At the end of the experiment, cells were digested from the membrane and blank membrane permeability was obtained. Blank permeability was measured at the end of the experiment, rather than prior to seeding, because any deposition or coating of albumin to the blank membrane would prevent cells from adhering later on. Permeability data for each day was then normalized to blank measurements and plotted over time (Fig. 5g).

Model toxin

Puromycin aminonucleoside (PAN, Sigma-Aldrich) was administered in solution with culture media to differentiated podocytes for 24 hours prior to permeability measurement (Fig. 6a and b) or cell harvesting for qPCR (Fig. 6c–e). Doses of 17 μM , 50 μM , and 100 μM were administered and compared to an untreated control group^{31,42} (Fig. 6d). The dose-response was conducted on cells differentiated in what we found to be a highly upregulated group: topographic platform, seeding density of 15 000 cells per cm^2 , and in ATRA-supplemented media. The high dose of PAN was also administered in the DEX media group to confirm the ability of the system to accurately capture the protective effects of the glucocorticoid (Fig. 6e).

Statistical analysis

Normality and equality of variance were tested using both SigmaPlot 12 and JMP 9. Two-way ANOVA or one-way ANOVA followed by pairwise comparisons with Fisher LSD method were used to determine the statistical significance and assess the interactive effects of factors in Fig. 2–4 and 6c–e. In the permeability studies in Fig. 5 and 6, Welch's *t*-tests were performed between groups on each day, allowing for unequal variances of the flat and bubble conditions. One-way repeated measures ANOVA tests were performed on the permeability data of each group to assess the time effect.

Results and discussion

Design of a biomimetic bubble platform

We designed and built a substrate covered with a micro-hemispherical topography, intended to mimic the curved capillaries of the glomerulus (Fig. 1a–c). Our approach incorporated a third-party material, spherical glass beads, during photolithography to impart microcurvature over a substrate. Glass beads were sprinkled on a layer of SU-8 and cured to the silicon wafer after exposure to UV light (Fig. 1d). The result was a master mold consisting of a topography of micro-hemispheres. By molding the master twice with PDMS soft lithography, we could replicate the microhemispherical mold to create biomimetic topographic PDMS substrates, hereafter

referred to as “bubble substrates” (Fig. 1e). These PDMS bubble substrates were fit into the wells of a 24-well cell culture plate and used with standard culture techniques.

In vivo, typical glomerular capillary diameter for rats is in the range of 7–11 μm , while the capillary loop length ranges around $72 \pm 38 \mu\text{m}$,^{43,44} where the capillary loop length represents the interval at which capillaries coil in the glomerulus. The substrate's bubble structures protrude at an average of 8 μm tall and 40 μm wide, which approximately suits the lower range of *in vivo* geometries, although not as narrow (Fig. 1f). The system also reflects the variability of capillary looping intervals by virtue of the random settling of glass beads during fabrication, which resulted in a distribution of structure dimensions (Fig. 1g and h). The end result is a substrate which captures the shape effects across a slice of the 3D spherical glomerulus, presenting that 3D structure across a 2D surface. This results in an effect like a 2 $\frac{1}{2}$ -dimensional representation of the glomerular microenvironment; a “slice of glomerulus.”

Many advanced engineered podocyte and kidney microenvironments use microfluidic channels to mimic the small dimensions of the nephron, since generating sophisticated biophysical microenvironments in larger formats has been a challenge.^{21,35,45–47} Our approach to microfabricating curvature effectively distributes the microhemispherical topography over any large surface area, making it applicable to both microfluidic and plate-based technologies. By applying the technology to the multi-well plate, we combine the benefits of standardized plate-based cell culture with those of more advanced culture systems, and provide a sophisticated alternative to microfluidic podocyte culture. It is a simple, fast, and highly repeatable approach for generating microscale curvature. Other methods for fabricating curvature in the micro scale have been reported in the literature, including: partial curing of photoresist to create arrays of cone-like features;⁴⁸ using thin polydimethylsiloxane (PDMS) membranes with applied vacuum to generate curved channels,⁴⁹ employing textile technology,⁵⁰ reflowing of positive photoresists,⁵¹ micromilling⁵² and deep-reactive-ion-etching.^{53,54} Our approach, using glass beads as a template in a modified form of photolithography, circumvents the need for multiple lengthy steps and for photo-masks, which dramatically decreases costs and processing time. It also provides a natural distribution of feature dimensions. This mold was used with PDMS as well as with hot embossing polystyrene, thereby demonstrating the versatility of the technology to scalable manufacturing (Fig. S1†).

Chemical and topographic cues interact to induce nephrin gene upregulation and protein expression

In vivo, podocytes have an arborized morphology with interdigitated foot processes that wrap around globular capillaries (Fig. 1a–c). The cell–cell contacts that line this network of interdigitated processes are rich in nephrin proteins, encoded by the NPHS1 gene.⁵⁵ Nephrin is central to the slit diaphragm complex, which provides barrier function in podocyte filtration. It is thus a specific marker of podocyte

maturity and lineage, and ought to be abundant in differentiated cells.^{1,56} However, appreciable levels of nephrin gene expression have been a challenge to maintain *in vitro*, which brings into question the lineage of those cells and their validity as podocyte models, especially since loss of nephrin expression correlates with a loss of glomerular filter integrity.⁵⁷

Treatment of culture media with biochemical supplements has previously been reported to upregulate nephrin expression. We formulated a culture media consisting of DMEM-F12 basal medium, 10% FBS, 1% pen-strep, with and without the addition of supplements including dihydroxy-vitamin D3 (Vit D3),^{58–60} all-trans retinoic acid (ATRA),³⁰ and dexamethasone (DEX).³¹ We were interested to see how topographic stimulation from our substrate would compare with advanced biochemical stimulation. Conditionally immortalized murine podocytes (E11) were cultured on either flat or bubble substrates, and in either unsupplemented or supplemented culture media, at differentiation conditions (38 °C) for 9 days, before beginning analysis (Fig. 2a).

Comparing results of nephrin gene expression, we confirmed that biochemical supplementation and topography both had a significant effect on upregulating gene expression, but in different ways (Fig. 2). Biochemical stimulation alone increased gene expression by several orders of magnitude, whereas topographic stimulation alone barely achieved a two-fold increase. However, there was a strong interaction effect between biochemical and topographic stimulation, such that the additional benefit of topography became dramatic when supplemented culture media were used. We observed that the addition of topography to a condition with one or more biochemical supplements had the same or greater effect on upregulating NPHS1 as did the addition of another biochemical supplement. For example, cultures stimulated with ATRA and topography were able to match or exceed gene expression levels that were attained with stimulation by ATRA plus DEX. Topography on top of ATRA plus DEX led to even further upregulation. This effect was consistent across both low and high cell seeding densities (Fig. 2b and c).

Thus, nephrin gene upregulation could be modulated by both chemical and physical means, and these stimuli may be interchanged while still maintaining higher levels of gene expression. This provides the opportunity to study different functions at higher expression levels than previously possible in well-plate cultures. For example, cultures supplemented with DEX lead to the highest gene expression levels. However, DEX treatment makes podocytes resistant to the effects of puromycin aminonucleoside (PAN), which is commonly used to induce a disease model.^{61–63} This would preclude studying this injury model at that level of expression. By using topography, we may circumvent the need for DEX as an additive while still maintaining the same high levels of gene expression for the model. Similarly, topography could simply be used to augment whatever maximum expression levels were achieved by biochemical means alone.

In addition to transcriptional profiling, we performed a Western blot assay to confirm the presence of full size ~180

kDa nephrin proteins (Fig. S6†). We detected ~180 kDa nephrin in both flat and bubble conditions with DEX-supplemented media, with a trend towards upregulation in the topographic group. We also identified multiple smaller fragments of nephrin in the immunoblot.^{64–66} Thus, various post-translational events may be occurring between the gene expression and protein expression stages, suggesting that protein expression patterns may be more nuanced *in vitro*, and would require more careful consideration when aiming to assess the functional properties of cultured cells.

Topographical and biochemical stimulation influences nephrin protein localization

While the presence of nephrin is important for confirming the identity of podocytes, and because it is a necessary component of slit diaphragms, without its localization to cell extremities it serves no functional purpose.⁵⁵ Nephrin is a transmembrane protein in the slit diaphragm that bridges between adjacent interdigitated foot processes. Defects in the nephrin protein or in its assembly to the slit diaphragm may become fatal, leading to conditions such as albuminuria, edema, malnutrition and increased risks of infection, as the compositional balance of the blood and urine is thrown off.⁶⁷ Proper structure and formation of slit diaphragms with correct nephrin localization is necessary to prevent passage of large molecules from the blood into urine. Thus, we were particularly interested in studying the location of nephrin proteins throughout the cell.

Consistent with nephrin gene expression, nephrin immunostaining confirmed protein expression in differentiated cells (Fig. 3a and S2†). While a fluorescence quantification of nephrin staining revealed comparable amounts of total nephrin in all groups, which may be associated with the smaller nephrin fragments identified by Western blotting (Fig. S3a and S6†), there was a marked change in protein arrangement. In response to either type of stimulation (*i.e.* topography or biochemical supplementation with DEX), nephrin stains changed from being faintly diffused throughout the entire cell body (– –), to being brightly localized in narrow regions in between adjacent cells, far from their nuclei (– +, + –, + +). This altered distribution is confirmed with a ratio of the nephrin stain located in the peripheral cytoplasm *versus* near the cell center (relative to the nucleus) (Fig. 3b and S3b†). A high ratio suggests that nephrin is shuttling to the cell extremities, where it should be located in a mature cell. Due to the presence of fragmented forms of nephrin for podocytes *in vitro*, supplementing protein quantification with localization analysis in this way may be a necessary step in more effectively elucidating *in vitro* functional nephrin organization.

Bubble-based geometric control over cell spatial organization

Bubble and flat substrates also differed in the spatial distribution of nephrin and cell body arrangement (Fig. 3c). Unique to the bubble platform, nephrin tended to extend up

over the curved bubble structures, while cell nuclei would fall to the valley regions in between protruding bubbles (Fig. 3d). Quantification of immunofluorescent staining from confocal images revealed that essentially 100% of nuclei within the field of view were located in the valleys (Fig. 3e and S4a†). Over half of the nephrin within the field of view was located on the bubble structures (Fig. 3f and S4b†), even though the majority (>60%) of the cell culture substrate was in fact flat valley area (Fig. 1f). A further comparison of the nephrin coverage showed that about 15% of the surface of bubble structures was covered with nephrin, while only about 5% of valley areas had nephrin coverage (Fig. 3g and S4c†). Together, we infer from these results that topography may guide how the cell arranges itself within its environment, where cell processes tend towards curved regions and cell bodies remain in valley regions (Fig. 4d, cartoon).

Cytoskeletal branching and process development

Podocyte function is extremely dependent on its form.³ A common pathological mechanism in kidney injury is foot process effacement, whereby the fine finger-like structure of foot processes retracts and becomes rounded, and actin fibers which are normally enriched in processes lose their branching distribution.^{7,24,68} The high complexity of the carefully arranged actin fibers in a branched and interdigitated process network is required for podocytes to be able to withstand the harsh glomerular environment, with incoming blood flow accounting for 25% of cardiac output.^{69,70} Having observed functional hallmarks of podocyte maturation such as upregulated nephrin gene expression and protein localization to cell boundaries, we next sought to assess the effects of topography on the structure of actin and cell processes that are so integral to podocyte morphology.

Podocytes have bundled actin stress fibers, which reorganize and begin to splay as foot processes form.^{71,72} These fibers are concentrated in foot processes, linking to the slit diaphragm and participating in sophisticated slit diaphragm signaling dynamics.^{32,68,72–76} We used confocal microscopy to visualize F-actin in our experiments (Fig. 4a and S5†). In a non-stimulated group (–), podocyte actin fibers were tightly packed and aligned linearly (Fig. 4a). Subtle clustering of actin into smaller strands was observed on the top and bottom edges of cells. Upon addition of either biochemical (– +) or topographical stimulation (+ –), actin fibers dramatically changed from linear and packed, to radially spread, with curved portions, overlapping edges, and more distinct clustering of fibers into several fanned-out strands. The combination of both types of stimuli (+ +) revealed the same radial network. These results suggest the development of a more advanced cytoskeletal structure. This progression into a more radial cytoskeletal structure is consistent with the literature, where stretch and flow stimulation lead to similar results.^{21,32,35,36}

To confirm the formation of finer process structures, we used scanning electron microscopy (SEM). We observed cell boundaries with protruding processes and in some cases

branching and interdigitation (Fig. 4b, arrows, and Fig. S7d†). This behaviour was not observed in mesenchymal stem cells, whose cytoplasmic extensions were also quantified as an additional control (Fig. S7†). Our observations of process branching and interdigitation in podocytes are important as they suggest early foot process development compared to filopodial activity.^{77,78} Processes were often found to overlap with each other, where process tips would be inserted under the adjacent cell's boundary. Unique to the bubble platform, cell processes also formed suspensions between adjacent bubble structures (Fig. 4c). Such suspensions appeared to be under significant tension, resonating with the need for cells to form strong cytoskeletal connections in their functional state.

To quantify cytoplasmic extensions on a cell boundary with protruding processes, we measured the length of the cell boundary across protrusions (boundary length) and the length when wrapping around the protruding processes (digitated length) (Fig. 4d). By taking the ratio of these two measurements, we could compare process formation per unit of cell boundary length (Fig. 4e). We found that topography significantly increased the digitation ratio in both supplemented and non-supplemented media conditions, while media supplements in fact had no significant effect on process digitation. This suggests that biophysical cues are a key component in the development of fine processes.

We also performed these measurements on SEM images of *in vivo* podocytes taken from the literature,^{39,40,79–81} and compared them with our experimental groups. While podocytes on flat substrates were always significantly below the digitation ratio found *in vivo*, podocytes on topographic substrates met or exceeded *in vivo* levels, suggesting that there is a sweet spot for the extent of process formation. Indeed, by comparing the average length of each process (Fig. 4f) and the number of fine processes per unit length (Fig. 4g), we found that cultured cells remain sparser than *in vivo*, and in some cases longer. Thus, it may be inferred that in a proper interdigitated podocyte network, foot processes might be slightly shorter and more densely packed together.

Thin membranes with controlled topography for studies of barrier function

Upon glomerular injury, podocytes, which are incapable of regenerative cell replication, typically undergo detachment, hypertrophy, and foot process effacement, leading to an overall breakdown in the ability to maintain the filtration barrier.⁸² The burden of filtration load becomes very high, resulting in proteinuria, where massive amounts of proteins such as albumin that ought to be retained in the blood end up passing through the glomerulus. These large quantities are unable to be reabsorbed by the tubules, causing stress and imbalance in downstream function. Clinically, even proteinuria greater than 1 g per day has been found to be the strongest risk factor for end stage kidney failure.^{8,83–87} Thus,

barrier function measured by retention of proteins is a functional property that should be able to be probed in a useful *in vitro* podocyte model.

To probe barrier function across a podocyte layer, it was necessary to translate our bubble substrate to a membrane-based system. Although microfluidic chambers are highly compatible with custom membranes due to the smaller surface area requirements,⁸⁸ we sought to develop a large-scale topographic membrane that could be applied to a transwell system, in order to remain compatible with the footprint and infrastructure of standardized well-plate technologies. Although various custom membranes for tissue engineering applications have been developed,⁸⁹ the fabrication of thin, permeable membranes with patterned microtopography has been limited. Microscale surface modification on membranes has been achieved with microcontact printing-based techniques,^{90,91} but the application to permeability studies is less common. Other techniques that incorporate porosity for permeability applications use photolithography and soft lithography to generate arrays of microholes, but these thin porous membranes are typically flat and do not feature out-of-plane microcurvature.^{92–96}

We developed a novel method for fabricating large-area, thin, porous, and micropatterned membranes for cell culture and permeability applications (Fig. 5). By pressing a gelled SU-8 layer with our desired bubble topography, then patterning pillars in the negative space, we created a thin mold that would yield our desired topography with patterned microholes in it (Fig. 5a). This mold could be used with either injection molding techniques (Fig. S8†), or with spin-coating, to apply and cure the final membrane material. The final result is a “topomembrane,” with the bubble topography and arrays of microholes (Fig. 5b). To prepare the custom membranes for cell culture, we replaced the membrane of a transwell insert with our topomembrane and used it with standard transwell culture techniques in a 24-well plate (Fig. 5c). Cells cultured on the topomembranes formed a confluent layer (Fig. 5d) and were differentiated for over 14 days for permeability studies (Fig. 5e).

Cells were cultured without biochemical supplementation on either flat or topomembranes, to probe the effect of topography alone on podocyte barrier function. Fluorescent albumin was added to the ‘blood’ side compartment and its transfer to the ‘urine’ compartment was measured (Fig. 5f). We took repeated measurements of albumin transfer across the podocyte layer, in an undifferentiated state (day 0), and during the cell differentiation process after 7 and 14 days of culture (Fig. 5g). By 14 days, the cells should have transitioned from proliferative to differentiated states.

Overall, topographic cultures tended to be more effective at blocking albumin diffusion across the membrane, even though the topomembrane has a higher overall surface area that cells need to attach to and cover due to the topography. Each insert was normalized to its own ‘blank’ permeability throughout the duration of the experiment, to account for the different baseline (blank) permeabilities of individual flat

and topomembranes. On day 14, the effect of topography on improving the podocytes’ barrier function, measured as a decrease in albumin transfer, became significant. Furthermore, although both groups limit albumin transfer compared to the membrane without cells, podocytes growing on the topomembrane had a significant improvement in performance with increasing differentiation time, as indicated by a reduction in albumin transfer compared to their undifferentiated (day 0) permeability (table in Fig. 5g). Flat cultures did not show significant improvements after differentiation time, even though both flat and bubble groups began with approximately equivalent undifferentiated permeability. This suggests that the differentiation process unfolds differently in the two groups. Although functional slit diaphragms are unlikely to be fully formed, the observed effects on reduced albumin transfer may be associated with closer cell-cell contacts, albumin uptake,²⁰ and higher cytoplasmic process branching and interdigitation, which may be contributing to more effective area coverage and therefore more efficient reductions of albumin transfer. The cumulative result suggests the topomembrane may present a more favourable microenvironment for encouraging functional podocyte assembly and study. Similarly, the variance in samples cultured on flat membranes was much larger than the variance of results from experiments on the topomembrane, suggesting that flat cultures may be more susceptible to nuisance factors such as concentration gradients, convection, or minor transformations, leading to less uniform results in permeability.

PAN-induced injury models

The success of an *in vitro* model depends on how closely it may approximate native properties, both healthy and pathologic. Modeling disease and injury can provide insight on pathogenesis as well as potential methods for treatment.⁹⁷ Further, understanding *in vitro* responses during injury can elucidate the path towards what should be healthy development, which can often be a challenge to discern when introducing new factors to *in vitro* microphysiological systems.^{98–101}

We studied the response of podocytes on puromycin aminonucleoside (PAN) injury in both topomembrane and bubble substrate systems, to check whether the systems were capable of capturing effects of injury. PAN is a podocyte toxin that is used to induce nephropathy *in vivo* and *in vitro*, with responses of proteinuria and DNA damage.^{61–63} To probe barrier function and the proteinuric response to injury, we used the topomembrane system. Podocytes were grown on flat and topomembranes in non-supplemented culture media for 14 days, then were injured with 100 μ M PAN for 24 hours (Fig. 6a and b). The bubble substrate was used to detect effects on relative gene expression, and cells were cultured for 9 days on the bubble substrate (Fig. 6c), with media supplemented with ATRA to observe the injury response (Fig. 6d), or with media supplemented with DEX to observe the protective effects of the glucocorticoid³¹ (Fig. 6e).

By employing both topomembrane and bubble substrate systems for our studies of injury, we were able to discern nuances in cell responses. Permeability tended to increase in response to PAN, and although the effects were not highly significant, the data suggests that the bubble group had a more acute response (Fig. 6b). Delving further into the bubble group's response, gene expression quantification did reveal significant effects on downregulating nephrin gene expression in a dose-dependent manner (Fig. 6d), suggesting that an early response to PAN injury begins with altering gene expression on the nanoscale before it may be felt by the microscale functions of podocytes. Furthermore, the bubble substrate system was able to correctly demonstrate the protective effects of DEX on podocytes against PAN-induced injury, where we observed resistance to the nephrin gene downregulation (Fig. 6e). Overall, the topographic system was capable of detecting nuanced changes relevant for toxicity studies.

Topography promotes higher-fidelity podocyte phenotype

In the native glomerulus, podocytes must maintain a sophisticated structure from the molecular arrangement of its protein complexes, to the patterning of its processes, and across the entire shape of its branching body. Cell bodies containing nuclei are often found in the folds between adjacent capillaries, with primary processes extending out radially in all directions, hooking between two capillaries. The cell is pulled in tension as it interlocks itself with other cells across capillaries, thus holding itself in place against the colossal forces of blood flow and filtration. These native features are in coherence with the *in vitro* observations from our topographic system. We observed the tendency of nuclei to reside in valleys between protruding curves, with processes branching across the tops of bubble structures to meet with adjacent cells and form digitated boundaries. Branching of the actin cytoskeleton and stress fiber formation went hand-in-hand with nephrin upregulation and localization. We observed radial spreading and formation of processes with interdigitation, even forming suspensions between adjacent bubbles—an effect that is not possible in other culture systems. Overall, the biomimetic effort of providing the physical shape underlying the 3D network of podocytes promoted responses that more closely resemble native features. The curvature may also affect these functions by imparting tension as cells wrap around curved features in 3D, bending actin-skeletal distributions, promoting stronger cell-cell and cell-bubble connections, or altering integrin patterning.

Conclusions

We have observed that biomimetic curved microtopography significantly promoted podocyte differentiation *in vitro*, and that the system was capable of detecting nuanced responses, both from microphysiological cues intended to promote differentiation, as well as from injury compounds that have the reverse effect. Both biochemical and biophysical

stimulation improved podocyte phenotype. While the effects on gene expression upregulation and on cytoskeletal rearrangement and protein clustering may be obtained by either topographic or biochemical means, topography did act as a superlative to biochemical stimulation. It also induced its own distinct effects on promoting the development of fine process protrusions, and on controlling cell spatial arrangement—the consequences of which remain to be further studied. These subtle differences between the two types of stimuli and the presence of their interaction effect suggest that fine tuning both would lead to more physiologically relevant *in vitro* models. We demonstrated the application of our bubble technology in both a 24-well plate system and in a transwell membrane system, which made readouts of gene expression, Western blot, immunofluorescent staining, SEM, and permeability all easily obtainable, and viable for toxicity studies. The accessibility of the methods we have developed for applying our topography to standard *in vitro* culture equipment makes it a relevant tool for enhancing current podocyte cultures, and we suggest its potential utility for the engineering of other tissue types with a curved native environment. Additional developments to the system could include co-cultures with fenestrated glomerular endothelium, and better approximation of the substrate's molecular surface to components of the glomerular basement membrane. These steps would further enhance the milieu towards creating an *in vitro* model of tripartite glomerular filtration, all while remaining within the simple footprint of a well plate.

Author contributions

A. K., B. Z., and M. R. conceived and designed the platform principle. A. K., B. Z., C. L., M. R., E. H., and C. J. contributed to methodology. A. K., B. Z., C. L., C. V., N. S., I. G., and S. A. contributed to investigation and analysis. A. K., B. Z., and N. S. wrote the manuscript. M. R., B. Z., E. H., C. J., and R. W. supervised the work and edited the manuscript. All authors discussed and commented on the manuscript and approved of its content.

Conflicts of interest

There are no conflicts to declare.

Acknowledgements

This work was made possible by the Natural Sciences and Engineering Research Council of Canada (NSERC) Steacie Fellowship to M. R., Alexander Graham Bell Canada Graduate Scholarships-Doctoral Program awarded to A. K., and the CIHR Banting Postdoctoral Fellowship to B. Z. This work was funded by the NSERC Collaborative Research and Development Grant (CRDPJ 5011), by the Canadian Institutes of Health Research (CIHR) Operating Grants (MOP-126027 and

MOP-137107), NSERC Discovery Grant (RGPIN 326982-10), and NIH grant 2R01 HL076485. We also thank Vivian Dai for her contributions in data analysis, and Andrea Lam for her animation and illustration work.

References

- H. Pavenstädt, W. Kriz and M. Kretzler, Cell Biology of the Glomerular Podocyte, *Physiol. Rev.*, 2003, **83**, 253.
- R. E. Botti, M. A. Razzak, W. J. MacIntyre and W. H. Pritchard, The Relationship of Renal Blood Flow to Cardiac Output in Normal Individuals as Determined by Concomitant Radioisotopic Measurements, *Cardiovasc. Res.*, 1968, **2**, 243–246.
- C. Schell and T. B. Huber, The Evolving Complexity of the Podocyte Cytoskeleton, *J. Am. Soc. Nephrol.*, 2017, **28**, 3166–3174.
- W. Kriz, I. Shirato, M. Nagata, M. LeHir and K. V. Lemley, The podocyte's response to stress: the enigma of foot process effacement, *Am. J. Physiol.*, 2012, **304**, F333–F347.
- K. Tryggvason and J. Patrakka, Thin Basement Membrane Nephropathy, *J. Am. Soc. Nephrol.*, 2006, **17**, 813–822.
- J. H. Miner, The Glomerular Basement Membrane, *Exp. Cell Res.*, 2012, **318**, 973.
- W. Kriz, Podocyte is the major culprit accounting for the progression of chronic renal disease, *Microsc. Res. Tech.*, 2002, **57**, 189–195.
- K. V. Lemley, *et al.* Podocytopenia and disease severity in IgA nephropathy, *Kidney Int.*, 2002, **61**, 1475–1485.
- CDC. Educational Resources | Publications & Resources | Chronic Kidney Disease Initiative | CDC. (2018). Available at: <https://www.cdc.gov/kidneydisease/publications-resources/educational-resources.html>. (Accessed: 29th March 2018).
- NIDDK, *Kidney Disease Statistics for the United States*, 2016.
- e-Statistics On Organ Transplants, Waiting Lists And Donors | CIHI. (2017). Available at: <https://www.cihi.ca/en/e-statistics-on-organ-transplants-waiting-lists-and-donors>. (Accessed: 14th May 2018).
- Organ Donation and Transplantation Statistics. National Kidney Foundation (2014). Available at: <https://www.kidney.org/news/newsroom/factsheets/Organ-Donation-and-Transplantation-Stats>. (Accessed: 14th May 2018).
- S. Y. Kim and A. Moon, Drug-induced nephrotoxicity and its biomarkers, *Biomol. Ther.*, 2012, **20**, 268–272.
- F. Ghane Shahrabaf and F. Assadi, Drug-induced renal disorders, *J. Renal Inj. Prev.*, 2015, **4**, 57–60.
- V. B. Siramshetty, *et al.* WITHDRAWN—a resource for withdrawn and discontinued drugs, *Nucleic Acids Res.*, 2016, **44**, D1080–D1086.
- P. S. Jat, *et al.* Direct derivation of conditionally immortal cell lines from an H-2Kb-tsA58 transgenic mouse, *Proc. Natl. Acad. Sci. U. S. A.*, 1991, **88**, 5096–5100.
- T. Ohse, *et al.* Establishment of Conditionally Immortalized Mouse Glomerular Parietal Epithelial Cells in Culture, *J. Am. Soc. Nephrol.*, 2008, **19**, 1879–1890.
- M. A. Saleem, *et al.* A conditionally immortalized human podocyte cell line demonstrating nephrin and podocin expression, *J. Am. Soc. Nephrol.*, 2002, **13**, 630–638.
- N. Jones, *et al.* Nck adaptor proteins link nephrin to the actin cytoskeleton of kidney podocytes, *Nature*, 2006, **440**, 818–823.
- B. Song, *et al.* The directed differentiation of human iPS cells into kidney podocytes, *PLoS One*, 2012, **7**, e46453.
- S. Musah, *et al.* Mature induced-pluripotent-stem-cell-derived human podocytes reconstitute kidney glomerular-capillary-wall function on a chip, *Nat. Biomed. Eng.*, 2017, **1**, 0069.
- O. Ciampi, *et al.* Generation of functional podocytes from human induced pluripotent stem cells, *Stem Cell Res.*, 2016, **17**, 130–139.
- S. Chittiprol, P. Chen, D. Petrovic-Djergovic, T. Eichler and R. F. Ransom, Marker expression, behaviors, and responses vary in different lines of conditionally immortalized cultured podocytes, *Am. J. Physiol.*, 2011, **301**, F660–671.
- J. Reiser and S. Sever, Podocyte Biology and Pathogenesis of Kidney Disease, *Annu. Rev. Med.*, 2013, **64**, 357–366.
- D. Schiwek, *et al.* Stable expression of nephrin and localization to cell-cell contacts in novel murine podocyte cell lines, *Kidney Int.*, 2004, **66**, 91–101.
- S. J. Shankland, J. W. Pippin, J. Reiser and P. Mundel, Podocytes in culture: past, present, and future, *Kidney Int.*, 2007, **72**, 26–36.
- Y. Takano, *et al.* Recovery and maintenance of nephrin expression in cultured podocytes and identification of HGF as a repressor of nephrin, *Am. J. Physiol.*, 2007, **292**, F1573–1582.
- M. Li, *et al.* Three-dimensional podocyte-endothelial cell co-cultures: Assembly, validation, and application to drug testing and intercellular signaling studies, *Eur. J. Pharm. Sci.*, 2016, **86**, 1–12.
- L. A. Bruggeman, R. P. Doan, J. Loftis, A. Darr and A. Calabro, A cell culture system for the structure and hydrogel properties of basement membranes; Application to capillary walls, *Cell Mol. Bioeng.*, 2012, **5**, 194–204.
- M. R. Vaughan, *et al.* ATRA induces podocyte differentiation and alters nephrin and podocin expression in vitro and in vivo, *Kidney Int.*, 2005, **68**, 133–144.
- R. F. Ransom, N. G. Lam, M. A. Hallett, S. J. Atkinson and W. E. Smoyer, Glucocorticoids protect and enhance recovery of cultured murine podocytes via actin filament stabilization, *Kidney Int.*, 2005, **68**, 2473–2483.
- N. Endlich, *et al.* Podocytes Respond to Mechanical Stress In Vitro, *J. Am. Soc. Nephrol.*, 2001, **12**, 413–422.
- A. T. Petermann, *et al.* Mechanical stress reduces podocyte proliferation in vitro, *Kidney Int.*, 2002, **61**, 40–50.
- M. Hu, *et al.* A biomimetic gelatin-based platform elicits a pro-differentiation effect on podocytes through mechanotransduction, *Sci. Rep.*, 2017, **7**, 43934.
- M. Zhou, *et al.* Development of a Functional Glomerulus at the Organ Level on a Chip to Mimic Hypertensive Nephropathy, *Sci. Rep.*, 2016, **6**, 31771.

- 36 C. Friedrich, N. Endlich, W. Kriz and K. Endlich, Podocytes are sensitive to fluid shear stress in vitro, *Am. J. Physiol.*, 2006, **291**, F856.
- 37 A. Ron, *et al.* Cell shape information is transduced through tension-independent mechanisms, *Nat. Commun.*, 2017, **8**, 2145.
- 38 A. Korolj, E. Y. Wang, R. A. Civitarese and M. Radisic, Biophysical stimulation for in vitro engineering of functional cardiac tissues, *Clin. Sci.*, 2017, **131**, 1393–1404.
- 39 K. Ichimura, *et al.* Morphological process of podocyte development revealed by block-face scanning electron microscopy, *J. Cell Sci.*, 2017, **130**, 132–142.
- 40 K. Ichimura, *et al.* Three-dimensional architecture of podocytes revealed by block-face scanning electron microscopy, *Sci. Rep.*, 2015, **5**, 8993.
- 41 M.-F. Hsu, *et al.* Protein tyrosine phosphatase Shp2 deficiency in podocytes attenuates lipopolysaccharide-induced proteinuria, *Sci. Rep.*, 2017, **7**, 461.
- 42 N. Guan, J. Ding, J. Deng, J. Zhang and J. Yang, Key molecular events in puromycin aminonucleoside nephrosis rats, *Pathol. Int.*, 2004, **54**, 703–711.
- 43 J. R. Nyengaard, Number and dimensions of rat glomerular capillaries in normal development and after nephrectomy, *Kidney Int.*, 1993, **43**, 1049–1057.
- 44 M. Steinhausen, *et al.* Intraglomerular microcirculation: measurements of single glomerular loop flow in rats, *Kidney Int.*, 1981, **20**, 230–239.
- 45 Z. Li, *et al.* Assessment of cadmium-induced nephrotoxicity using a kidney-on-a-chip device, *Toxicol. Res.*, 2017, **6**, 372–380.
- 46 X. Mu, W. Zheng, L. Xiao, W. Zhang and X. Jiang, Engineering a 3D vascular network in hydrogel for mimicking a nephron, *Lab Chip*, 2013, **13**, 1612.
- 47 K. J. Jang, *et al.* Human kidney proximal tubule-on-a-chip for drug transport and nephrotoxicity assessment, *Integr. Biol.*, 2013, **5**, 1119–1129.
- 48 M. Li, *et al.* Microarchitecture for a three-dimensional wrinkled surface platform, *Adv. Mater.*, 2015, **27**, 1880–1886.
- 49 J. Y. Park, D. H. Lee, E. J. Lee and S.-H. Lee, Study of cellular behaviors on concave and convex microstructures fabricated from elastic PDMS membranes, *Lab Chip*, 2009, **9**, 2043–2049.
- 50 V. Hosseini, *et al.* Fiber-assisted molding (FAM) of surfaces with tunable curvature to guide cell alignment and complex tissue architecture, *Small*, 2014, **10**, 4851–4857.
- 51 T. Thorsen, S. J. Maerkl and S. R. Quake, Microfluidic Large-Scale Integration, *Science*, 2002, **298**, 580.
- 52 J. Z. Yu, E. Korkmaz, M. I. Berg, P. R. LeDuc and O. B. Ozdoganlar, Biomimetic scaffolds with three-dimensional undulated microtopographies, *Biomaterials*, 2017, **128**, 109–120.
- 53 J. C. H. Poon, *et al.* Design of biomimetic substrates for long-term maintenance of alveolar epithelial cells, *Biomater. Sci.*, 2018, **6**, 292–303.
- 54 C. J. Bettinger, B. Orrick, A. Misra, R. Langer and J. T. Borenstein, Microfabrication of poly (glycerol–sebacate) for contact guidance applications, *Biomaterials*, 2006, **27**, 2558–2565.
- 55 M. Kestilä, *et al.* Positionally cloned gene for a novel glomerular protein–nephrin—is mutated in congenital nephrotic syndrome, *Mol. Cell*, 1998, **1**, 575–582.
- 56 T. Benzing, Signaling at the Slit Diaphragm, *J. Am. Soc. Nephrol.*, 2004, **15**, 1382–1391.
- 57 J. Patrakka and K. Tryggvason, Nephrin – a unique structural and signaling protein of the kidney filter, *Trends Mol. Med.*, 2007, **13**, 396–403.
- 58 R. Agarwal, Vitamin D, proteinuria, diabetic nephropathy, and progression of CKD, *Clin. J. Am. Soc. Nephrol.*, 2009, **4**, 1523–1528.
- 59 O. Trohatou, E.-F. Tsilibary, A. Charonis, C. Iatrou and G. Drossopoulou, Vitamin D3 ameliorates podocyte injury through the nephrin signalling pathway, *J. Cell. Mol. Med.*, 2017, **21**, 2599–2609.
- 60 X. L. Zhang, Y. F. Guo, Z. X. Song and M. Zhou, Vitamin D prevents podocyte injury via regulation of macrophage M1/M2 phenotype in diabetic nephropathy rats, *Endocrinology*, 2014, **155**, 4939–4950.
- 61 V. Sanwal, *et al.* Puromycin Aminonucleoside Induces Glomerular Epithelial Cell Apoptosis, *Exp. Mol. Pathol.*, 2001, **70**, 54–64.
- 62 C. B. Marshall, J. W. Pippin, R. D. Krofft and S. J. Shankland, Puromycin aminonucleoside induces oxidant-dependent DNA damage in podocytes in vitro and in vivo, *Kidney Int.*, 2006, **70**, 1962–1973.
- 63 M. Rico, *et al.* WT1-interacting protein and ZO-1 translocate into podocyte nuclei after puromycin aminonucleoside treatment, *Am. J. Physiol.*, 2005, **289**, F431–441.
- 64 D. P. K. Ng, *et al.* Nephriuria associates with multiple renal traits in type 2 diabetes, *Nephrol., Dial., Transplant.*, 2011, **26**, 2508–2514.
- 65 A. Pätäri, *et al.* Nephriuria in Diabetic Nephropathy of Type 1 Diabetes, *Diabetes*, 2003, **52**, 2969–2974.
- 66 V. Ruotsalainen, *et al.* Nephrin is specifically located at the slit diaphragm of glomerular podocytes, *Proc. Natl. Acad. Sci. U. S. A.*, 1999, **96**, 7962–7967.
- 67 (a) S. Ranganathan, Pathology of Podocytopathies Causing Nephrotic Syndrome in Children, *Front. Pediatr.*, 2016, **4**, 32; (b) W. Y. Ding and M. A. Saleem, Current concepts of the podocyte in nephrotic syndrome, *Kidney Res. Clin. Pract.*, 2012, **31**, 87–93.
- 68 F.-F. He, S. Chen, H. Su, X.-F. Meng and C. Zhang, Actin-associated Proteins in the Pathogenesis of Podocyte Injury, *Curr. Genomics*, 2013, **14**, 477–484.
- 69 G. S. Pazhayattil and A. C. Shirali, Drug-induced impairment of renal function, *Int. J. Nephrol. Renovasc. Dis.*, 2014, **7**, 457–468.
- 70 M. Dixit, T. Doan, R. Kirschner and N. Dixit, Significant Acute Kidney Injury Due to Non-steroidal Anti-inflammatory Drugs: Inpatient Setting, *Pharmaceuticals*, 2010, **3**, 1279–1285.
- 71 K. Ichimura, H. Kurihara and T. Sakai, Actin Filament Organization of Foot Processes in Rat Podocytes, *J. Histochem. Cytochem.*, 2003, **51**, 1589–1600.

- 72 C. Faul, K. Asanuma, E. Yanagida-Asanuma, K. Kim and P. Mundel, Actin up: regulation of podocyte structure and function by components of the actin cytoskeleton, *Trends Cell Biol.*, 2007, **17**, 428–437.
- 73 T. Lu, *et al.* HIV-1 Nef Disrupts the Podocyte Actin Cytoskeleton by Interacting with Diaphanous Interacting Protein, *J. Biol. Chem.*, 2008, **283**, 8173–8182.
- 74 P. Mundel and S. J. Shankland, Podocyte biology and response to injury, *J. Am. Soc. Nephrol.*, 2002, **13**, 3005–3015.
- 75 L. A. New, *et al.* Nephric Tyrosine Phosphorylation Is Required to Stabilize and Restore Podocyte Foot Process Architecture, *J. Am. Soc. Nephrol.*, 2016, **27**, 2422–2435.
- 76 P. Mundel, *et al.* Rearrangements of the cytoskeleton and cell contacts induce process formation during differentiation of conditionally immortalized mouse podocyte cell lines, *Exp. Cell Res.*, 1997, **236**, 248–258.
- 77 J. Kreidberg and A. Podocyte, Differentiation and Glomerulogenesis, *J. Am. Soc. Nephrol.*, 2003, **14**, 806–814.
- 78 F. Kliewe, *et al.* Studying the role of fascin-1 in mechanically stressed podocytes, *Sci. Rep.*, 2017, **7**, 9916.
- 79 Y. Yu, C.-G. Leng, N. Terada and S. Ohno, Scanning electron microscopic study of the renal glomerulus by an in vivo cryotechnique combined with freeze-substitution, *J. Anat.*, 1998, **192**, 595–603.
- 80 J. H. Suh, G. Jarad, R. G. VanDeVoorde and J. H. Miner, Forced expression of laminin beta1 in podocytes prevents nephrotic syndrome in mice lacking laminin beta2, a model for Pierson syndrome, *Proc. Natl. Acad. Sci. U. S. A.*, 2011, **108**, 15348–15353.
- 81 T. Burghardt, *et al.* Advanced electron microscopic techniques provide a deeper insight into the peculiar features of podocytes, *Am. J. Physiol.*, 2015, **309**, F1082–1089.
- 82 A. M. Davison, *Oxford textbook of clinical nephrology*, Oxford University Press, 2005.
- 83 L. Huan, L. Yuezong, W. Chao and T. HaiTao, The urine albumin-to-creatinine ratio is a reliable indicator for evaluating complications of chronic kidney disease and progression in IgA nephropathy in China, *Clinics*, 2016, **71**, 243–250.
- 84 K. Kamei, *et al.* Proteinuria during Follow-Up Period and Long-Term Renal Survival of Childhood IgA Nephropathy, *PLoS One*, 2016, **11**, e0150885.
- 85 M. W. Taal and B. M. Brenner, Predicting initiation and progression of chronic kidney disease: Developing renal risk scores, *Kidney Int.*, 2006, **70**, 1694–1705.
- 86 B. Haraldsson, J. Nystrom and W. M. Deen, Properties of the glomerular barrier and mechanisms of proteinuria, *Physiol. Rev.*, 2008, **88**, 451–487.
- 87 S. Agrawal, A. J. Guess and M. A. Chanley, Smoyer & William, E. Albumin-induced podocyte injury and protection are associated with regulation of COX-2, *Kidney Int.*, 2014, **86**, 1150–1160.
- 88 D. Huh, *et al.* Microfabrication of human organs-on-chips, *Nat. Protoc.*, 2013, **8**, 2135–2157.
- 89 (a) E. T. Baran, K. Tuzlakoglu, A. Salgado and R. L. Reis, Microchannel-patterned and heparin micro-contact-printed biodegradable composite membranes for tissue-engineering applications, *J. Tissue Eng. Regen. Med.*, 2011, **5**, e108–e114; (b) E. M. Frohlich, *et al.*, Topographically-patterned porous membranes in a microfluidic device as an in vitro model of renal reabsorptive barriers, *Lab Chip*, 2013, **13**, 2311–2319; (c) H. Zong, *et al.*, Designing function-oriented artificial nanomaterials and membranes via electrospinning and electrospaying techniques, *Mater. Sci. Eng., C*, 2018, **92**, 1075–1091; (d) R. N. Carter, *et al.*, Ultrathin transparent membranes for cellular barrier and co-culture models, *Biofabrication*, 2017, **9**, 015019.
- 90 X. Shi, *et al.* Stretchable and Micropatterned Membrane for Osteogenic Differentiation of Stem Cells, *ACS Appl. Mater. Interfaces*, 2014, **6**, 11915–11923.
- 91 P. Camelliti, J. O. Gallagher, P. Kohl and A. D. McCulloch, Micropatterned cell cultures on elastic membranes as an in vitro model of myocardium, *Nat. Protoc.*, 2006, **1**, 1379.
- 92 K. Takoh, T. Ishibashi, T. Matsue and M. Nishizawa, Localized chemical stimulation of cellular micropatterns using a porous membrane-based culture substrate, *Sens. Actuators, B*, 2005, **108**, 683–687.
- 93 J. Ou, C. L. Ren and J. Pawliszyn, A simple method for preparation of macroporous polydimethylsiloxane membrane for microfluidic chip-based isoelectric focusing applications, *Anal. Chim. Acta*, 2010, **662**, 200–205.
- 94 K. Takoh, A. Takahashi, T. Matsue and M. Nishizawa, A porous membrane-based microelectroanalytical technique for evaluating locally stimulated culture cells, *Anal. Chim. Acta*, 2004, **522**, 45–49.
- 95 D. Tahk, *et al.* Rapid large area fabrication of multiscale through-hole membranes, *Lab Chip*, 2017, **17**, 1817–1825.
- 96 D. Huh, *et al.* Reconstituting Organ-Level Lung Functions on a Chip, *Science*, 2010, **328**, 1662–1668.
- 97 B. Zhang, A. Korolj, B. F. L. Lai and M. Radisic, Advances in organ-on-a-chip engineering, *Nat. Rev. Mater.*, 2018, **3**, 257–278.
- 98 A. van de Stolpe and J. den Toonder, Workshop meeting report Organs-on-Chips: human disease models, *Lab Chip*, 2013, **13**, 3449–3470.
- 99 M. E. Andersen, *et al.* Developing Microphysiological Systems for Use as Regulatory Tools – Challenges and Opportunities, *ALTEX*, 2014, **31**, 364–367.
- 100 S. Ahadian, *et al.* Organ-On-A-Chip Platforms: A Convergence of Advanced Materials, Cells, and Microscale Technologies, *Adv. Healthcare Mater.*, 2017, **7**, 1700506.
- 101 Y. Zhao, A. Korolj, N. Feric and M. Radisic, Human pluripotent stem cell-derived cardiomyocyte based models for cardiotoxicity and drug discovery, *Expert Opin. Drug Saf.*, 2016, **15**, 1455–1458.